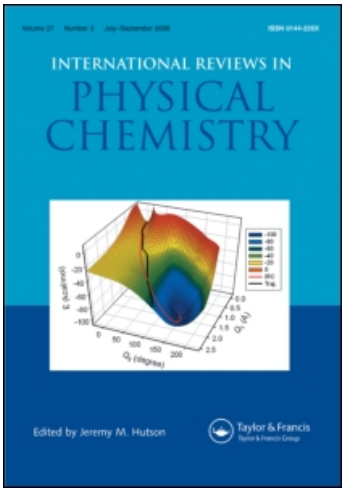

International Reviews in Physical Chemistry
Publication details, including instructions for authors and subscription information:
http://www.informaworld.com/smpp/title~content=t713724383

Molecular collisions in ultracold atomic gases

Jeremy M. Hutson[a]; Pavel Soldán[a]
[a] Department of Chemistry, University of Durham, Durham, DH1 3LE, England

To cite this Article Hutson, Jeremy M. and Soldán, Pavel(2007) 'Molecular collisions in ultracold atomic gases', International Reviews in Physical Chemistry, 26: 1, 1 — 28
To link to this Article: DOI: 10.1080/01442350601084562
URL: http://dx.doi.org/10.1080/01442350601084562

International Reviews in Physical Chemistry,
Vol. 26, No. 1, January–March 2007, 1–28

Taylor & Francis
Taylor & Francis Group

Molecular collisions in ultracold atomic gases

JEREMY M. HUTSON*† and PAVEL SOLDÁN‡

†Department of Chemistry, University of Durham, South Road,
Durham, DH1 3LE, England
‡Doppler Institute, Department of Physics, Faculty of Nuclear Sciences
and Physical Engineering, Czech Technical University, Břehová 7,
115 19 Praha 1, Czech Republic

(*Received 22 June 2006; in final form 10 October 2006*)

It has recently become possible to form molecules in ultracold gases of trapped alkali metal atoms. Once formed, the molecules may undergo elastic, inelastic and reactive collisions. Inelastic and reactive collisions are particularly important because they release kinetic energy and eject atoms and molecules from the trap. The theory needed to handle such collisions is presented and recent quantum dynamics calculations on ultracold atom–diatom collisions of spin-polarized $Li + Li_2$, $Na + Na_2$ and $K + K_2$ are described. All these systems have potential energy surfaces on which barrierless atom exchange reactions can occur, and both inelastic and reactive rates are very fast (typically $k_{inel} > 10^{-10}\,cm^3\,s^{-1}$ in the Wigner regime).

Contents

*Corresponding author. j.m.hutson@durham.ac.uk

International Reviews in Physical Chemistry
ISSN 0144–235X print/ISSN 1366–591X online
http://www.tandf.co.uk/journals
DOI: 10.1080/01442350601084562

1. Introduction

There have been enormous recent advances in our ability to produce and trap samples of cold molecules (below 1 K) and ultracold molecules (below 1 mK). Molecules such as NH_3, OH and NH have been cooled from room temperature to the milli-Kelvin regime by a variety of methods including buffer-gas cooling [1, 2] and Stark deceleration [3, 4]. Molecules have also been produced in ultracold atomic gases by photoassociation [5, 6] and magnetoassociation [5, 7] of pairs of atoms. Long-lived molecular Bose–Einstein condensates have been produced for dimers of fermionic alkali metal atoms [8–10], and the first signatures of ultracold triatomic [11] and tetraatomic [12] molecules have been observed.

Cold and ultracold molecules have many possible applications. High-resolution spectroscopy on cold molecules may allow the measurement of fundamental physical properties such as the electric dipole moment of the electron [13], the energy differences between enantiomers [14, 15] and the time-dependence of the fine-structure constant [16]. In addition, since molecules have a much richer energy level structure than atoms, they offer many new possibilities for quantum control. Perhaps most importantly, *dipolar* molecules interact with one another much more strongly and at longer range than atoms. Dipolar molecules have been proposed as qubits for quantum computers [17] and dipolar quantum gases are predicted to exhibit a range of novel features [18].

In a recent article [5], we reviewed the current state of the art of molecule production in ultracold atomic gases. Other authors have reviewed the cooling of molecules from near room temperature [3, 4] and the theory of collisions of such directly cooled molecules [19–21]. The present article is complementary to these and focusses on recent theoretical work on the collisions of alkali metal dimers formed in ultracold gases.

2. Experiments on ultracold molecule formation and collisions

There are two main methods used to form molecules in ultracold atomic gases. In *photoassociation* [5, 6], a pair of atoms undergoes a spectroscopic transition from an unbound atomic state very close to threshold to a bound molecular state. In *magneto-association*, also known as *Feshbach resonance tuning* [5, 7], the transition is accomplished by guiding the atom pair adiabatically across an avoided crossing between an unbound state and a molecular state.

Feshbach resonance tuning always produces molecules in very highly excited states, usually the highest vibrational state that exists in the diatomic potential well. Photoassociation also usually produces molecules in very high vibrational states,

because they are the ones that have the best Franck–Condon overlap with the free-atom states.

Ultracold molecules are initially formed in the presence of ultracold atoms and can collide with them. For molecules in vibrationally excited states, there is the possibility of vibrationally inelastic collisions,

$$M_2(v) + M \longrightarrow M_2(v' < v) + M, \tag{1}$$

where v is the vibrational quantum number. Since the trap depth is usually much less than 1 K, such collisions always release enough kinetic energy to eject both collision partners from the trap. If the molecular density is high, there is also the possibility of inelastic molecule–molecule collisions,

$$M_2(v) + M_2(v) \longrightarrow M_2(v' < v) + M_2(v'' \leq v). \tag{2}$$

Molecules are not *destroyed* in inelastic collisions, but they are lost from the trap and are no longer ultracold.

The initial experiments on molecule formation by Feshbach resonance tuning worked with bosonic isotopes of alkali metals [22–25]. They found that the molecules were lost from the trap on a timescale of milliseconds. The loss was attributed to vibrationally inelastic atom–molecule collisions with relaxation rates around $10^{-10}\,\mathrm{cm^3\,s^{-1}}$. For the case of $^{85}Rb_2$ [22], recent work has suggested that the loss may in fact be due to spontaneous molecular dissociation by collisionless spin relaxation [26, 27]. However, for the other systems [23–25] the molecules are formed in truly bound states and cannot decay without collisions. Mukaiyama *et al.* [28] have recently measured the trap loss rate for $^{23}Na_2$ molecules formed by Feshbach resonance tuning and obtained an atom–molecule rate coefficient $k_{\mathrm{loss}} = 5.1 \times 10^{-11}\,\mathrm{cm^3\,s^{-1}}$ for molecules in the highest vibrational state.

Fermion dimers formed by Feshbach resonance tuning are a very special case. In mid-2003, four groups independently reported within a very short time that dimers of fermionic ^{6}Li [29–31] and ^{40}K [32] could be remarkably stable to collisions. Cubizolles *et al.* [30] and Jochim *et al.* [31] showed that the lifetime was particularly large close to a Feshbach resonance, where the atom–atom scattering length is large and positive. By the end of 2003, three different groups [8–10] had succeeded in creating long-lived molecular Bose–Einstein condensates of fermion dimers.

Petrov *et al.* [33, 34] analysed the stability of fermion dimers in terms of the long-range form of the wavefunction. In the case where the atom–atom scattering length a is much larger than the range of the atom–atom potential r_e, they showed that both atom–molecule and molecule–molecule inelastic collision rates are suppressed by Fermi statistics. However, their derivation applies only to molecules that are in long-range states, with a wavefunction that depends on the scattering length a, $\chi(r) \sim \exp(-r/a)$. As will be discussed in more detail below, Cvitaš *et al.* [35] have shown computationally that there is *no* systematic suppression of the atom–molecule inelastic rate for fermion dimers in low-lying vibrational levels, even when a is large and positive.

Relaxation processes have also been studied for molecules formed by photoassociation. Wynar *et al.* [36] formed $^{87}Rb_2$ molecules in the second-to-last vibrational level of the ground excited state by stimulated Raman adiabatic passage (STIRAP). They estimated an upper bound of $k_{\rm loss} = 8 \times 10^{-11}\,{\rm cm^3\,s^{-1}}$ due to inelastic atom–molecule collisions. Staanum *et al.* [37] investigated inelastic collisions of rovibrationally excited Cs_2 ($^3\Sigma_u^+$) in collisions with Cs atoms in two different ranges of the vibrational quantum number v by monitoring trap loss of Cs_2. They obtained atom–molecule rate coefficients close to $1.0 \times 10^{-10}\,{\rm cm^3\,s^{-1}}$ for both $v = 4$ to 6 and $v = 32$ to 47. Zahzam *et al.* [38] carried out similar work for different rovibrational states of $^3\Sigma_u^+$, and also considered molecules in the $^1\Sigma_g^+$ state and molecule–molecule collisions. They obtained rate coefficients of $2.6 \times 10^{-11}\,{\rm cm^3\,s^{-1}}$ and $1.0 \times 10^{-11}\,{\rm cm^3\,s^{-1}}$ in the atom–atom and atom–molecule cases respectively, both with quite large error bounds.

Because of the collisional losses for excited vibrational levels, intense efforts are under way to produce ultracold alkali metal dimers in low-lying levels (and ultimately in the ground vibronic state). The process of transferring molecules from atomic or near-dissociation molecular states, with probability density at long range, to low-lying states, with probability density near the diatomic equilibrium distance r_e, is sometimes called *r*-transfer. It can in principle be achieved either by using many photons to accomplish the transfer in several stages [39] or by using tailored ultrafast laser pulses [40–42]. In favourable cases, and particularly for heteronuclear alkali metal dimers [43, 44], it may be possible to produce molecules in their vibrational ground state by two-photon processes via excited states with mixed singlet and triplet character. Sage *et al.* [45] have recently succeeded in creating ultracold RbCs molecules ($T \approx 100\,\mu{\rm K}$) in their vibronic ground state using a four-photon process. The production rate in the current experiments is only 500 molecules/s, but work is under way to increase it.

Inspired by the recent progress in experimental techniques for producing and studying ultracold molecules, we have collaborated with Jean-Michel Launay and coworkers at the University of Rennes to produce a series of theoretical studies [35, 46–52] on interactions and collisions between spin-polarized alkali-metal atoms and molecules. In particular, ultra-low-energy collisions were studied for $Na + Na_2$ [46, 48], $Li + Li_2$ (isotopically homonuclear [35, 49] and heteronuclear [50]), and $K + K_2$ [51]. Collisions between alkali-metal dimers and atoms present several new theoretical challenges that are not present for collisions of stabler molecules. The remainder of this review will focus on describing this work and drawing general conclusions from it.

3. General aspects of alkali metal dimer collisions

The atoms in an ultracold quantum gas of S-state atoms are in states labelled by the electron spin s, the nuclear spin i, and the total angular momentum f. Since there is usually a magnetic field present, the states are also labelled by m_f, the projection of f along the field. Of particular interest here are *spin-stretched* states, where $f = f_{\rm max} = i + s$ and $|m_f| = f$. From a theoretical point of view, collisions of atoms and molecules in spin-stretched states are simpler than others, because they take place entirely on high-spin potential energy surfaces. For alkali metal atoms with $s = \frac{1}{2}$, these are triplet curves

($S=1$) for atom–atom collisions and quartet surfaces ($S=\frac{3}{2}$) for atom–molecule collisions and three-body recombination. For atoms in non-spin-stretched states, singlet dimer curves and doublet trimer surfaces are also required. Our work so far has focussed on spin-stretched states.

The lowest quartet state of the alkali metal trimers, which correlates with ground-state atoms (^{2}S) and molecules in their lowest triplet state ($^3\Sigma_u^+$), is designated ($1^4A'$). At first sight it might be expected that three parallel electrons in s orbitals would not form significant chemical bonds. If this was the case, then *pairwise additivity* would be a good approximation and the potential energy surface would be given by

$$V(r_{12}, r_{23}, r_{13}) \approx \sum_{i<j}^{3} V_{\text{dimer}}(r_{ij}). \tag{3}$$

The potential energy curve for the lowest triplet state is reasonably well known for many of the alkali metal dimers [53–56]. Pairwise-additive model potentials have been extensively used in theoretical studies of three-body recombination [57–60].

As will be seen below, pairwise additivity is actually quite a poor approximation for the alkali metals. Nevertheless, it gives some insights into the energetics of atom–molecule collisions. If the dimer well depth is ε at an atom–atom distance r_e, then for a pairwise-additive surface the energies of various important arrangements of three atoms are

- atom M well-separated from diatom M_2 with bond length r_e,

$$V(\mathbf{r}) = V(r_e, \infty, \infty) = -\varepsilon$$

- linear trimer M_3 with bond length r_e,

$$V(\mathbf{r}) = V(r_e, r_e, 2r_e) \approx -2\varepsilon$$

- triangular trimer M_3 with bond length r_e,

$$V(\mathbf{r}) = V(r_e, r_e, r_e) = -3\varepsilon.$$

The topology of the lowest quartet potential energy surface of an alkali-metal trimer is thus quite simple; the global minimum is at an equilateral triangular configuration (point group D_{3h}) and there is a saddle point at a symmetric linear configuration ($D_{\infty h}$). The inclusion of non-additivity deepens the linear and (especially) triangular trimer wells, but does not change the overall conclusions.

The potential energy surfaces are such that *barrierless atom-exchange reactions* can occur. *All* configurations of the trimer M_3 are lower in energy than the separated atom + diatom collision partners (and products). Once the collision complex M_3 has been formed, any one of the three atoms can depart to form products. Even when the products are indistinguishable from the reactants, all three of these 'arrangement channels' must be taken into account in the collision dynamics. This has two

major consequences. First, a reactive scattering approach (rather than an inelastic scattering approach) must be used in the dynamics calculations. Secondly, the scattering calculations must be done on a fully three-dimensional potential energy surface. This is not the case for non-reactive scattering, where the products and reactants are confined to just one arrangement, and two-dimensional calculations (with the diatomic bond length kept fixed at the dimer equilibrium geometry) or quasi-three-dimensional calculations (where the diatomic bond length is varied only slightly around the dimer equilibrium geometry) are usually used.

The major focus of interest is in collisions that release kinetic energy and thus lead to trap loss. These are typically vibrational relaxation processes of the type

$$M_2(v) + M \longrightarrow M_2(v' < v) + M. \tag{4}$$

However, if the three atoms are identical it is not possible to distinguish between *inelastic* processes and *reactive* processes. We therefore use the general term *quenching* to describe collisions that produce a change in the vibrational (or rotational) quantum number and release kinetic energy.

4. Potential energy surfaces

4.1. *Non-additive forces*

Accurate quantum scattering calculations require accurate potential energy surfaces. Higgins *et al*. [61] showed in 2000 that the quartet state of Na_3 exhibits strong non-additive forces that increase the well depth of the equilateral trimer by 59% and decrease the Na-Na bond length from 5.2 Å in the triplet dimer to 4.4 Å in the quartet trimer. We therefore carried out a systematic study [47] to investigate such effects for the whole series of homonuclear alkali-metal trimers. *Ab initio* electronic structure calculations were performed using a single-reference restricted open-shell variant [62] of the coupled-cluster method [63] with single, double and non-iterative triple excitations [RCCSD(T)]. Medium/large-size basis sets were used for the alkali metal atoms as described in [47], and the full counterpoise correction of Boys and Bernardi [64] was employed to compensate for basis-set superposition errors. All the *ab initio* calculations were performed using the MOLPRO package [65].

The results are summarized in table 1, which shows the equilibrium bond lengths r_e and potential depths V_{min} for alkali-metal dimers and equilateral (D_{3h}) trimers, together with the corresponding quantities r_{sp} and V_{sp} for the linear ($D_{\infty h}$) saddle points. The three-body non-additive contributions V_3 are also given. Figure 1 shows the additive and non-additive potential energy curves for D_{3h} geometries.

All the trimers show quite strong non-additive effects. The quartet trimers all have equilibrium interatomic distances (at D_{3h} geometries) that are substantially shorter than those of the triplet dimers, by an amount that decreases down the series from 1.07 Å in Li_3 to 0.59 Å in Cs_3. The trimer potentials are all correspondingly deeper than pairwise sums of dimer potentials, by a factor of 1.3 to 1.5 for the heavier alkali metals (Na to Cs) but a factor of more than 4 for Li.

Table 1. RCCSD(T) values of r_e(Å), r_{sp}(Å), $V_{min} = -D_e(cm^{-1})$, $V_{sp}(cm^{-1})$, and $V_3(cm^{-1})$ for spin-polarized alkali dimers and trimers.

	Dimer		Trimer D_{3h}			Trimer $D_{\infty h}$		
	r_e	V_{min}	r_e	V_{min}	V_3	r_{sp}	V_{sp}	V_3
Li	4.169	−334.046	3.103	−4022	−5260	3.78	−968	−354
Na	5.214	−174.025	4.428	−837	−663	5.10	−381	−27
K	5.786	−252.567	5.084	−1274	−831	5.67	−569	−52
Rb	6.208	−221.399	5.596	−995	−513	6.13	−483	−15
Cs	6.581	−246.786	5.992	−1139	−562	6.52	−536	−32

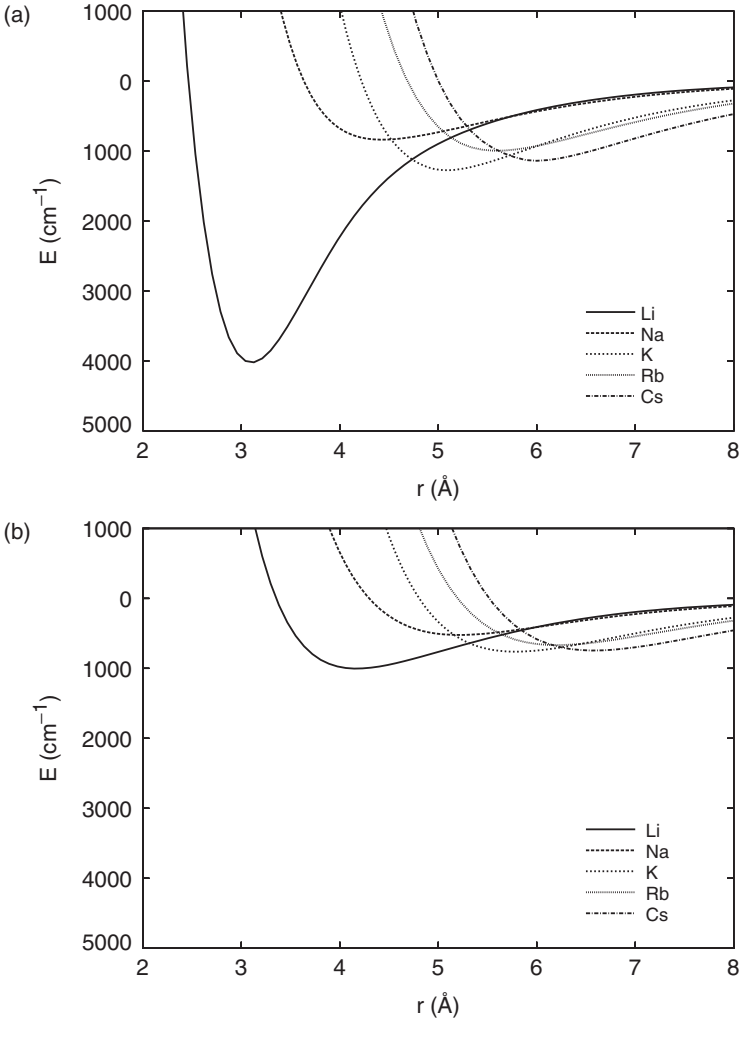

Figure 1. RCCSD(T) interaction energies of spin-polarized alkali trimers at D_{3h} geometries (a) full potentials including non-additive contributions; (b) additive potentials. Reproduced from Soldán *et al.* [47].

The size of the non-additivity is at first sight quite surprising in chemical terms. It contrasts with the situation for the rare gas trimers, where the non-additive contributions are only 0.5% to 2.5% [66, 67] and produce a *weakening* of the binding at equilateral geometries rather than a *strengthening* as in table 1.

The interaction potentials can be decomposed into self-consistent field (SCF) and correlation contributions. For the triplet alkali dimers, as for the rare gas dimers, the SCF potentials are repulsive and the main attractive forces arise from interatomic correlation (dispersion). However, this similarity does *not* extend to the trimers. For the rare gases, most of the non-additivity comes from the dispersion interaction. The leading long-range term in this is the Axilrod–Teller–Muto (ATM) triple-dipole term [68, 69], which is repulsive near equilateral configurations but attractive near linear configurations. For alkali metal atoms, by contrast, there is a large attractive contribution to the non-additive energy that exists even at the SCF level. This occurs because the alkali metals have vacant *n*p orbitals that lie relatively close to the *n*s orbitals.

The question then arises why the p orbitals contribute so strongly for the alkali metal trimers but not the dimers. Soldán *et al*. [47] carried out a natural orbital analysis for equilateral triangle geometries, and considered the contribution from *radial* p orbitals (pointing towards the centre of the triangle) and from *tangential* p orbitals (pointing around the ring). The radial p orbitals can form bonding and antibonding molecular orbitals (MOs) of the same symmetry as those formed from the *n*s orbitals (a_1' and e'), while the tangential p orbitals can form a_2' and e' MOs. The sets of MOs of the same symmetry interact, lowering the energy of the occupied MOs and contributing to bonding. Soldán *et al*. showed that the dominant contribution to the trimer bonding is from the tangential p orbitals. In chemical terms, this is essentially sp hybridization. This mechanism does not occur for the alkali metal dimers, because in that case the 'tangential' p orbitals form molecular orbitals of π symmetry that cannot mix with σ orbitals.

4.2. *Global potential energy surfaces*

It is relatively straightforward to generate potential energy surfaces for systems such as the quartet alkali metal trimers by carrying out *ab initio* electronic structure calculations at grids of points that sample the configuration space. We have carried out such calculations for Li_3 [35, 49] and K_3 [51], using RCCSD(T) calculations as described above for the linear and equilateral geometries. Colavecchia *et al*. [70] have also carried out calculations for Li_3, using a more complete treatment of the valence electron correlation (full configuration interaction) but without correlating the core electrons.

A much more difficult problem is to generate a global potential energy surface from a set of points. For quantum dynamics calculations, it is very important to represent the potential-energy function smoothly and without oscillations between *ab initio* points. If the resulting potential is to be capable of representing all the properties of experimental interest (including atom–atom scattering lengths, dimer and trimer bound states, atom–diatom collisions and three-body recombination), then it is very important that the potential should dissociate properly into all possible sets of products (atom + diatom and three separated atoms) with the correct long-range behaviour.

There are several coordinate systems that can be used for triatomic systems, including hyperspherical coordinates, Jacobi coordinates, and bond-length coordinates. These are by no means equivalent for interpolation purposes. In particular, grids of points in hyperspherical coordinates tend to include points in which two atoms lie very close together, which hinders interpolation because polynomials with very high localized maxima tend to have oscillations in other regions. Jacobi coordinates suffer from the same problem, and also do not allow the full three-body exchange symmetry to be introduced in a natural way. Fortunately, there is no need to represent the potential energy surface in the same coordinate system as is used in the dynamical calculations. We therefore chose to carry out electronic structure calculations on a grid of points in bond-length coordinates (r_{12}, r_{23}, r_{13}). We use the shorthand $(\mathbf{r})$ for this to simplify notation.

In order to represent the atom–diatom dissociation limits correctly, it is essential to use a long-range representation in which the triatomic potential is decomposed into a sum of additive and non-additive contributions,

$$V(\mathbf{r}) = \sum_{i<j}^{3} V_{\text{dimer}}(r_{ij}) + V_3(\mathbf{r}). \tag{5}$$

Provided $V_3(\mathbf{r}) \to 0$ when any two of the atom–atom distances become infinite, this guarantees that the correct diatomic potential is recovered in the atom–diatom limit. However, low-energy scattering is very sensitive to long-range forces, so we also require that the atom–diatom dispersion coefficients and their anisotropies are correctly reproduced. This requires careful treatment of the long-range part of $V_3(\mathbf{r})$.

An important point is that, for a pairwise-additive potential in which the dimer potentials have the correct long-range form $-C_6R^{-6}$, the atom–diatom C_6 coefficient is *isotropic* (independent of Jacobi angle θ). The anisotropy of the atom–diatom C_6 coefficient comes entirely from non-additive forces. Cvitaš *et al.* [52] have therefore investigated the relationships between three-body dispersion coefficients in the atom–diatom and atom–atom–atom representations and derived formulae relating the atom–diatom C_6 and C_8 coefficients and their anisotropies to three-body coefficients arising from triple-dipole [68, 69], quadruple–dipole [71, 72] and higher-order multipole [73, 74] terms.

A variety of representations can be used for interpolating dimer potentials. We have used the reciprocal-power reproducing kernel Hilbert space method (RP-RKHS) [75, 76]. With an appropriate choice of parameters [77], this gives a potential that has the correct C_6 and C_8 dispersion coefficients.

At short range, different approaches were needed for K_3 and for Li_3. K_3 is representative of the heavier alkali metals (Na to Cs) in that the non-additive potential is smaller than the potential itself for most configurations. It is thus convenient to use equation (5) directly with a global representation of $V_3(\mathbf{r})$. The details of the procedure are given in [51] and [52], but in brief:

- a quantity $V'_3(\mathbf{r})$ is defined by subtracting out damped versions of the triple-dipole and dipole–dipole–quadrupole terms from $V_3(\mathbf{r})$,

$$V'_3(\mathbf{r}) = V_3(\mathbf{r}) - \left[V^{\text{DDD}}_{3,\text{damp}}(\mathbf{r}) + V^{\text{DDQ}}_{3,\text{damp}}(\mathbf{r}) \right]; \tag{6}$$

- a function

$$g(\mathbf{r}) = \frac{r_{12}^3 r_{23}^3 r_{13}^3}{(1+\cos^2\phi_1)\, r_{23}^6 + (1+\cos^2\phi_2)\, r_{13}^6 + (1+\cos^2\phi_3)\, r_{12}^6} \tag{7}$$

  is defined to eliminate the quadruple–dipole contribution to $V_3(\mathbf{r})$;
- the function $V_3''(\mathbf{r}) = g(\mathbf{r}) \times V_3'(\mathbf{r})$ is interpolated using three-dimensional RP-RKHS interpolation. $V_3''(\mathbf{r})$ is suitable for this (but $V_3(\mathbf{r})$ and $V_3'(\mathbf{r})$ are not) because $V_3''(\mathbf{r})$ takes a product form at long range, constant $\times\, r_{12}^{-3} r_{23}^{-3} r_{31}^{-3}$;
- $V_3(\mathbf{r})$ is then rebuilt from $V_3''(\mathbf{r})$ at each interpolated point,

$$V_3(\mathbf{r}) = \frac{V_3''(\mathbf{r})}{g(\mathbf{r})} + \left[V_{3,\mathrm{damp}}^{\mathrm{DDD}}(\mathbf{r}) + V_{3,\mathrm{damp}}^{\mathrm{DDQ}}(\mathbf{r}) \right]. \tag{8}$$

The resulting potential energy surfaces for spin-polarized K_3 [51] are shown in figure 2. Note that the depth at D_{3h} geometries is rather more than twice that at linear geometries, whereas pairwise additivity would give a factor of 1.5.

Li_3 required a different procedure, because in this case the potential minimum for the trimer occurs at a distance that is high on the repulsive wall for the dimer. Because of this, equation (5) would represent the interaction potential in this region as a difference between two very large quantities. Nevertheless, at long range a decomposition according to equation (5) is essential. Under these circumstances, it is best to fit the *ab initio* points directly to obtain a short-range function $V_{\mathrm{SR}}(\mathbf{r})$ without imposing the correct long-range behaviour. A switching function $S(\mathbf{r})$ is then used to join this onto the correct long-range form,

$$V(\mathbf{r}) = S(\mathbf{r}) V_{\mathrm{SR}}(\mathbf{r}) + [1 - S(\mathbf{r})] V_{\mathrm{LR}}(\mathbf{r}). \tag{9}$$

The switching function is 1 at short range but switches smoothly to zero at long range. The long-range form $V_{\mathrm{LR}}(\mathbf{r})$ is designed to be valid when *any* of the atom–atom distances is large, and the procedure used to build in the correct three-atom and atom–diatom dispersion coefficients is described in [52].

A further complication arises for Li_3 because in this case there is a second potential energy surface involved. As described above, the quartet state that correlates with three ground-state (^{2}S) atoms has $^4A'$ symmetry ($^4\Sigma^+$ at linear geometries). The second state correlates with Li(^{2}S) + Li(^{2}S) + Li(^{2}P) and has $^4\Pi$ symmetry at linear geometries. It can cross the $^4\Sigma^+$ state at linear geometries because it has different symmetry. However, at non-linear geometries the $^4\Pi$ state splits into $^4A'$ and $^4A''$ components, and the two $^4A'$ states mix and cannot cross. There are thus *conical intersections* at linear geometries, and the avoided crossings produce double-minimum structures at non-linear geometries as shown in the upper panel of figure 3. The line of conical intersections produced a *seam* in the potential surface as shown in the lower panel.

Conical intersections exist for both symmetrical and unsymmetrical linear geometries in quartet Li_3, but for strongly unsymmetrical geometries the conical intersections are high on the repulsive wall and will not affect the dynamics. However, for near-symmetric linear geometries the seam dips to an energy of about $-100\,\mathrm{cm}^{-1}$

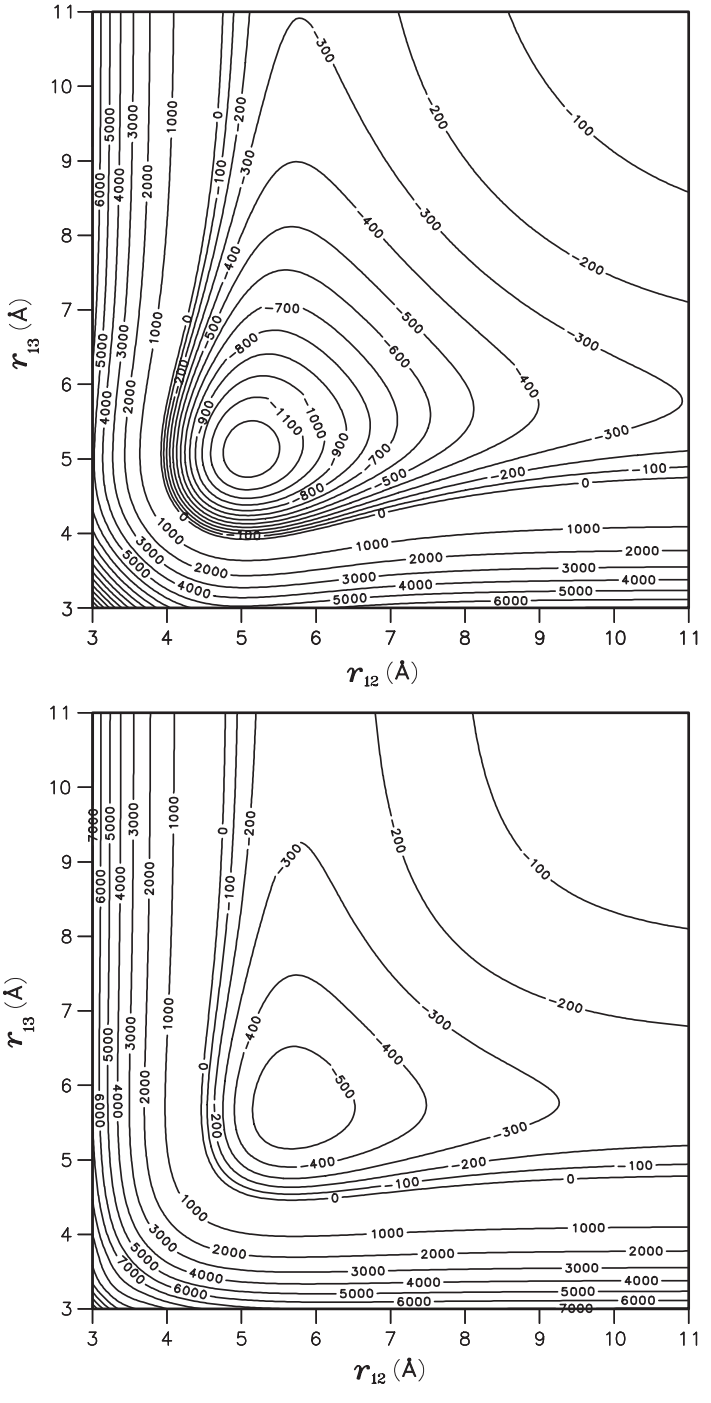

Figure 2. Cuts through the K_3 quartet surface in valence coordinates. Upper panel: cut for a bond angle of 60°, showing the global minimum at $-1269\,cm^{-1}$ and 5.09 Å. Lower panel: cut at collinear geometries; the collinear minimum is at $-565\,cm^{-1}$ and 5.68 Å. Contours are labelled in cm^{-1}. Reproduced from Quéméner *et al*. [51].

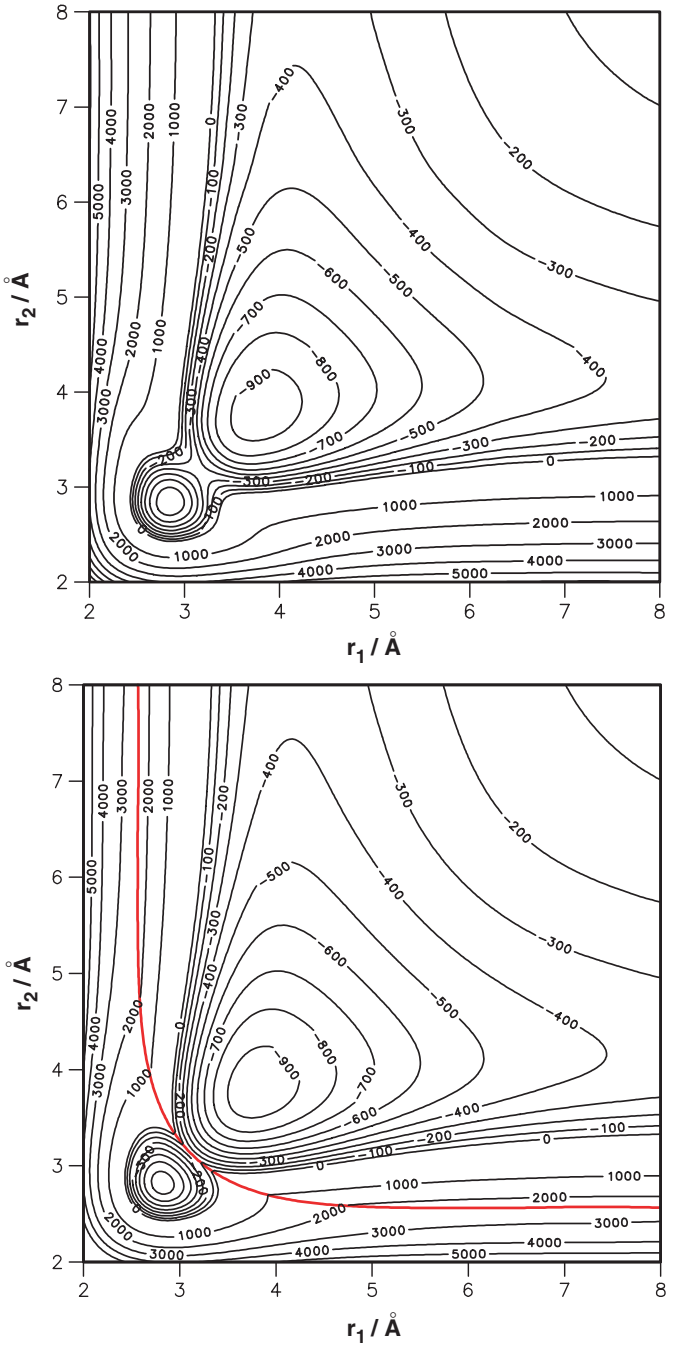

Figure 3. [Colour online] Cuts through the Li_3 quartet surface in valence coordinates. Upper panel: cut for a bond angle of 170°, showing the double-minimum structure due to avoided crossings at near-linear geometries. Lower panel: cut at collinear geometries, showing the seam of conical intersections (red line) between the $^4\Sigma^+$ and $^4\Pi$ states. Reproduced from Cvitaš *et al.* [35].

(relative to the energy of three free atoms) at $r_{12} = r_{23} \approx 3.1$ Å. It is thus close to the inner turning point for low-energy collisions between Li and Li_2, and may have significant consequences for the chemical dynamics. The conical intersection has subsequently been characterized in more detail by Brue *et al*. [78].

5. Quantum dynamics calculations

5.1. *Methodology*

As described above, alkali metal atom + diatom collisions require a fully reactive scattering treatment, and at the energies of interest for cold molecules it is essential to handle relative translation as well as internal motions quantum-mechanically. Quantum reactive scattering calculations [79] can in general be performed using either *time-dependent* or *time-independent* treatments. In recent work at higher energies, time-dependent treatments based on wavepacket dynamics have been becoming increasingly popular [80]. At ultralow energies, however, the time evolution of a wavepacket is very slow, and propagating it until it reaches the asymptotic region requires an impractical number of time steps. Furthermore, it is difficult to converge wavepacket calculations at very low scattering energies, because the wave packet needs to be very broad. We therefore chose to describe ultralow energy scattering in a *time-independent* formalism.

There are many variants of time-independent reactive scattering theory. However, some of them are unsuitable for the alkali metal trimers. As described above, the strong non-additive three-body interactions for the alkali metal trimers make the atom–atom distances at the trimer equilibrium geometry much shorter than those for the dimers. The vibrational wavefunctions of a free dimer are centred around its equilibrium bond length and are very small at the distances that correspond to the trimer equilibrium. Because of this, the free dimer wavefunctions do not form a good basis set for expanding the scattering wavefunctions in the region of the trimer equilibrium, where the actual atom exchange takes place. This precludes the use of standard reactive scattering packages such as the ABC program [81], which uses such basis functions and has been widely used in studies of reactions such as $F+H_2$ [82–84] and $O(^3P)+H_2$ [85] at ultralow energies.

We thus chose to use a scattering formalism based on hyperspherical coordinates ρ, θ, ϕ [86]: ρ is the hyperradius, which describes the size of the triangle formed by the three atoms, while θ and ϕ are hyperangles, which describe the shape of the triangle. Hyperspherical approaches do not use free-diatom functions as a basis set in the region of the trimer minimum. Instead, they define an adiabatic basis set by solving a fixed-ρ Schrödinger equation on a grid of values of the hyperradius ρ. There are several different hyperspherical approaches available. The approach developed for reactive scattering by Pack and Parker [87, 88] solves the angular problem using a finite-element approach in adiabatically adjusting principal axis hyperspherical (APH) coordinates and then solves the resulting radial coupled equations by propagation. The approach developed by Esry and coworkers [58, 89] and used extensively for three-body recombination in cold gases [58–60] solves the angular problem in slightly

modified Smith–Whitten coordinates [86] using basis splines and then handles the radial problem with a finite element approach. Both these methods use an optimized non-uniform grid in the hyperangles. However, we chose to use an alternative approach developed by Launay and LeDourneuf [90], which has been applied extensively to chemical reactions such as $N(^2D)+H_2$ [91] and $O(^1D)+H_2$ [92] at higher energies.

In the approach of Launay and LeDorneuf, the configuration space is divided into inner and outer regions, and the boundary between them is placed at a distance (hyperradius) such that couplings due to the residual atom–diatom interaction can be neglected outside the boundary. This distance is typically $\rho = 45$ to 60 a_0 for the alkali metal systems. In the inner region, the wavefunction for nuclear motion is obtained by propagating a set of coupled differential equations using a diabatic-by-sector algorithm. The angular basis set is obtained by diagonalizing a fixed-hyperradius reference Hamiltonian in a primitive basis set of pseudo-hyperspherical harmonics. In the outer region, the wavefunction is expanded in a basis set of diatom vibration–rotation functions expressed in Jacobi coordinates [93]. The wavefunctions in the outer region are computed by inwards integration of regular and irregular solutions of an uncoupled radial Schrödinger equation which includes the isotropic part of the atom–molecule interaction. Matching between wavefunctions for the inner and outer regions yields the scattering S-matrix. Elastic and inelastic cross sections are then calculated using standard formulae [51].

The size of the basis set required for convergence depends strongly on the masses involved and the depth of the potential energy well. Before our calculations on alkali metal systems, nearly all quantum scattering calculations had been on systems containing only one or occasionally two non-hydrogen atoms. Calculations on alkali metal atoms require much bigger angular basis sets, though fortunately at low energies only a few partial waves (values of J, the total angular momentum excluding spin) are needed. Even for $Li + Li_2$ [35], which is relatively light, the number of adiabatic angular functions retained in the coupled equations ranged from 97 for $J = 0$ to 827 for $J = 10$, while for $K + K_2$ [51] the range was from 250 for $J = 0$ to 1411 for $J = 5$.

One problem with hyperspherical methods is that the diatom functions become more localized in hyperangular space as ρ increases. Because of this, the number of hyperspherical harmonics needed for convergence increases with ρ: for $K + K_2$ it varied from 867 functions at small ρ to 6625 functions at the matching distance. It is the calculation to build the adiabatic angular basis that dominates the computer requirements (180 hours on an IBM Power4 P960 for $K + K_2$).

A major advantage of the hyperspherical harmonics is that boson or fermion symmetry is very easy to impose. The complete nuclear permutation group for a system with three identical nuclei is S_3. To satisfy the Pauli principle, the total wavefunction must have A_1 symmetry for bosonic nuclei or A_2 symmetry for fermionic nuclei. The total wavefunction is in general a sum of products of electronic, nuclear spin and nuclear motion parts. For three atoms in their spin-stretched states, the nuclear spin wavefunction is totally symmetric. For such states, collisions take place entirely on the quartet surface, for which the electronic wavefunction has A_2 symmetry. Boson or fermion symmetry can thus be imposed by selecting pseudo-hyperspherical harmonics to give the correct symmetry for the wavefunction for nuclear motion. The adiabatic states in each sector are obtained by a variational expansion on a basis of hyperspherical

harmonics with A_1 symmetry for bosonic atoms (with fermionic nuclei) and A_2 symmetry for fermionic atoms (with bosonic nuclei).

All the calculations were carried out on the quartet trimer surfaces, so are appropriate for collisions of spin-polarized atoms and molecules. However, the basis functions used for the quantum dynamics calculations did not explicitly include electron spin. In a more complete treatment, the rotational quantum number n for the triplet dimer would couple to its spin $s=1$ to give a resultant j. When spin is neglected, however, there is no distinction between n and j. The splittings between levels of the same n but different j are in any case very small for the alkali metal dimers.

5.2. *Homonuclear molecules*

Quantum dynamics calculations have been carried out for the homonuclear collisions Li + $Li_2(v=0$ to 3) [35, 49], $Na + Na_2(v=0$ to 3) [46, 48] and $K + K_2(v=1)$ [51]. For the Li and K systems, calculations were carried out for both bosonic and fermionic isotopes.

The results for Li are typical. Figures 4 and 5 show elastic and inelastic cross sections for bosons (^{7}Li) and fermions (^{6}Li) respectively. The elastic and inelastic s-wave cross sections for ^{7}Li are compared directly and extended to lower energy in figure 6. It may be seen that at very low energies (below 100 μK for Li) the elastic cross sections become independent of energy whereas the inelastic cross sections are proportional to $E_{\mathrm{kin}}^{-1/2}$. This is in accordance with the Wigner threshold laws, which state that at very low energy the partial cross sections (contributions from a single partial wave l) for elastic and inelastic scattering vary as

$$\sigma_{\mathrm{el}}^{l} \sim E_{\mathrm{kin}}^{2l}; \qquad \sigma_{\mathrm{inel}}^{l} \sim E_{\mathrm{kin}}^{l-1/2}. \tag{10}$$

For a long-range potential proportional to R^{-6}, as for neutral atom–diatom scattering, there is an l-independent term that dominates the threshold law for high l so that $\sigma_{\mathrm{el}}^{l} \sim E_{\mathrm{kin}}^{3}$ for $l \geq 2$ [94].

It may be seen from figures 4 and 5 that below $E_{\mathrm{kin}} = 100\,\mu\mathrm{K}$ the cross sections are completely dominated by the $l=0$ term, which corresponds to total angular momentum $J=0$ for bosons but $J=1$ for fermions (because $J = l + j$ and the lowest rotational level of a triplet fermion dimer is $j=1$). The energy-dependence of the inelastic rate coefficient is $k\sigma_{\mathrm{inel}}$ where $k = (2E_{\mathrm{kin}}/\mu)^{1/2}$, so that the inelastic rate is independent of energy in this region.

Above $E_{\mathrm{kin}} = 100\,\mu\mathrm{K}$, the $l=0$ contribution starts to deviate from the Wigner limit and higher partial waves start to contribute. The point at which this happens depends somewhat on mass, and is closer to 10 μK for $K + K_2$ [51].

As described in section 2, it is known experimentally that fermion dimers produced by Feshbach resonance tuning are very much stabler than boson dimers when the scattering length is large. This stability was crucial in the production of molecular Bose–Einstein condensates of $^6Li_2$ [8, 9] and $^{40}K_2$ [10]. Petrov *et al.* [33] explained the stability in terms of the requirements of Fermi–Dirac statistics. However, their

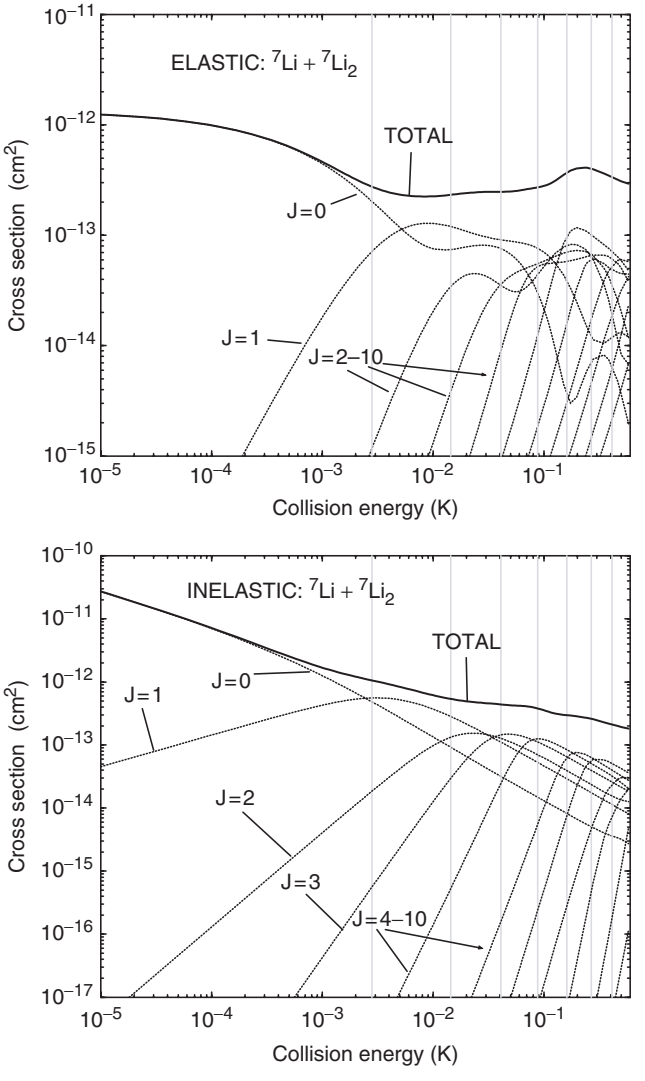

Figure 4. Elastic cross sections (upper panel) and inelastic cross sections (lower panel) for $^7Li + ^7Li_2(v_i = 1, j_i = 0)$, with contributions from individual partial waves (total angular momentum J, excluding spin). The vertical lines indicate centrifugal barrier heights for $l \geq 1$. Reproduced from Cvitaš *et al.* [35].

derivation is valid only for long-range molecular states. A very important question is whether the stability persists for low-lying vibrational states of fermion dimers.

Cvitaš *et al.* [35] carried out quantum dynamics calculations for spin-polarized collisions of ultracold homonuclear $Li + Li_2$ collisions for both the bosonic (^7Li) and fermionic (^6Li) cases. The results shown in figures 4 and 5 correspond to vibrational quenching rates for $v = 1$ of $k_{inel} = 5.6 \times 10^{-10}\,cm^3\,s^{-1}$ for bosons and $2.8 \times 10^{-10}\,cm^3\,s^{-1}$ for fermions. However, the apparent difference of a factor of 2 is not significant: there

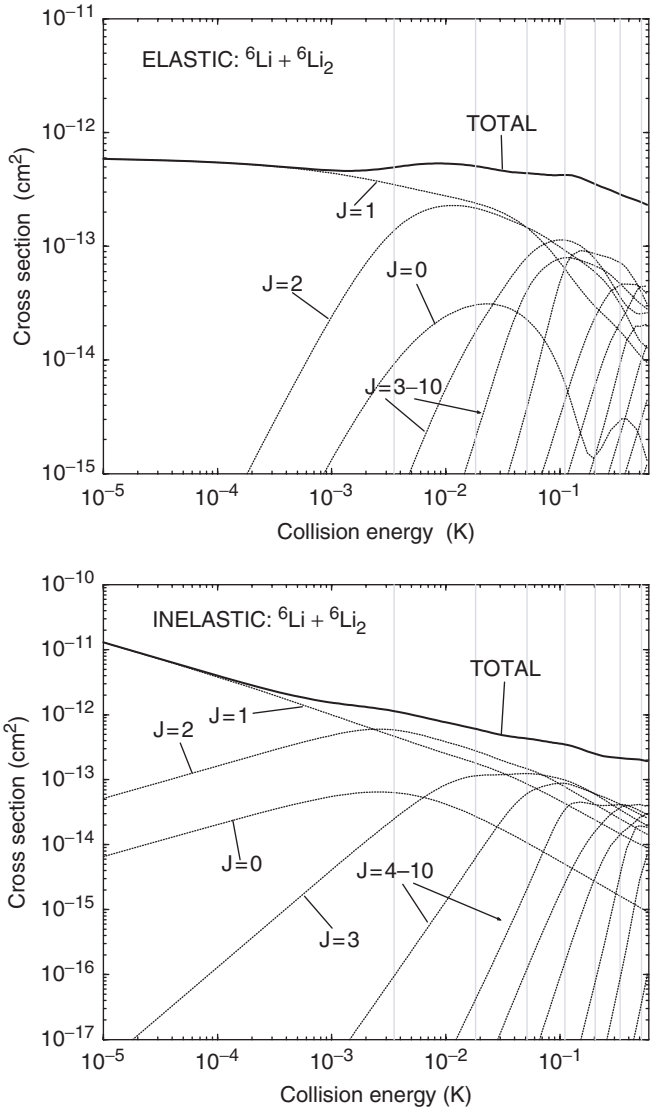

Figure 5. Elastic cross sections (upper panel) and inelastic cross sections (lower panel) for $^6Li + {}^6Li_2(v_i = 1, j_i = 1)$, with contributions from individual partial waves (total angular momentum J, excluding spin). The vertical lines indicate centrifugal barrier heights for $l \geq 1$. Reproduced from Cvitaš *et al.* [35].

were differences of up to a factor of 8 between inelastic cross sections for different initial values of v and j. Cvitaš *et al.* found no *systematic* difference between inelastic rates in the boson and fermion cases, even when the atom–atom scattering length was adjusted to be large and positive. This has important consequences for efforts to transfer the dimer population from Feshbach resonance states to the vibrational ground state, $v = 0$: it will be necessary to carry out the process either in a single step or quickly enough

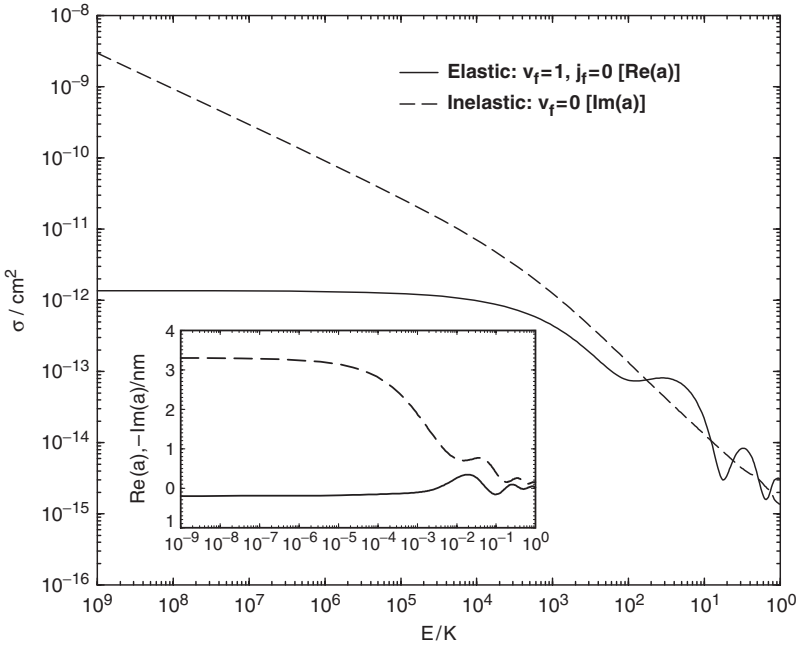

Figure 6. Elastic and inelastic s-wave ($J=0$) cross sections for $^7Li + {}^7Li_2(v_i=1, j_i=0)$. The inset shows the real and imaginary parts of the complex scattering length.

that the molecules do not spend enough time in intermediate states to undergo inelastic collisions.

The effective potential for a partial wave with $l > 0$ is governed at long range by the centrifugal and dispersion terms,

$$V^l(R) = \frac{\hbar^2 l(l+1)}{2\mu R^2} - \frac{C_6}{R^6}, \tag{11}$$

where C_6 is the atom–diatom dispersion coefficient. There is thus a centrifugal barrier at a distance

$$R^l_{\max} = \left[\frac{6\mu C_6}{\hbar^2 l(l+1)}\right]^{1/4} \tag{12}$$

with height

$$V^l_{\max} = \left[\frac{\hbar^2 l(l+1)}{\mu}\right]^{3/2} (54C_6)^{-1/2}. \tag{13}$$

The resulting barrier heights are included in figures 4 and 5. The first vertical line corresponds to the $l=1$ partial wave and so on up to the $l=7$ partial wave.

It may be seen that each partial cross section has a maximum at an energy slightly higher than the corresponding $V^l_{\max}$. At collision energies below the centrifugal barrier, the partial cross sections for each l follow Wigner laws given by equation (10). Above the centrifugal barrier, the inelastic probabilities come close to their maximum value of 1 and the cross sections vary as E^{-1} because of the k^{-2} factor in the expression for the cross section.

5.3. *Capture model outside the ultracold regime*

At high collision energy, when several partial waves are involved, the total inelastic rate coefficient can be compared with that given by the classical Langevin capture model [95], based on the idea that every collision that crosses the centrifugal barrier produces inelasticity. This gives

$$\begin{aligned} \sigma^{\text{capture}}_{\text{inel}}(E) &= 3\pi\left(\frac{C_6}{4E}\right)^{1/3}; \\ k^{\text{capture}}_{\text{inel}}(E) &= 3\pi\left(\frac{C_6}{4E}\right)^{1/3}\left(\frac{2E}{\mu}\right)^{1/2} = \frac{3\pi C_6^{1/3}E^{1/6}}{2^{1/6}\mu^{1/2}}. \end{aligned} \tag{14}$$

This rate coefficient is shown as a function of collision energy for $Li + Li_2$ in figure 7 and compared with the quenching rates for bosons and fermions initially in $v = 1$ and 2 [35]. It may be seen that the full quantum result approaches the Langevin value at collision energies above about 10 mK. Similar behaviour is seen for $K + K_2$ at collision energies above 0.1 mK [51].

5.4. *Product rotational distributions*

The vibrational spacings of the alkali metal dimers are much larger than their rotational spacings, so that many rotational levels are energetically accessible in collisions that cause vibrational relaxation. For Na_2, for example, rotational levels up to $j = 20$ are energetically accessible at the energy of the $v = 1$ state (23.5 cm^{-1}). All accessible levels are populated in the products, subject to symmetry restrictions (only even-j levels for bosons and odd-j levels for fermions). The product rotational distributions for $Na + Na_2$ ($v = 1$) at 10^{-4} K are shown in figure 8. There are three clear maxima in the distribution, at $j = 4$, 12 and 18. The oscillations probably arise from a rotational rainbow effect [96, 97]. The structure is similar to that observed in vibrational predissociation of Van der Waals complexes [98]. In a classical impulsive model, the energy released from Na_2 vibration is partly retained in relative translation and partly converted into Na_2 rotation. The angular momentum imparted to the Na_2 molecule is zero if the energy is released at a linear or T-shaped geometry, but large around $\theta = 45^\circ$. In this model, the oscillations arise from interference between classical trajectories on either side of the maximum.

The rotational distributions become constant at low energies but show structure above 10^{-4} K. This is shown for $K + K_2$ ($v = 1$) in figure 9. In this case levels up to

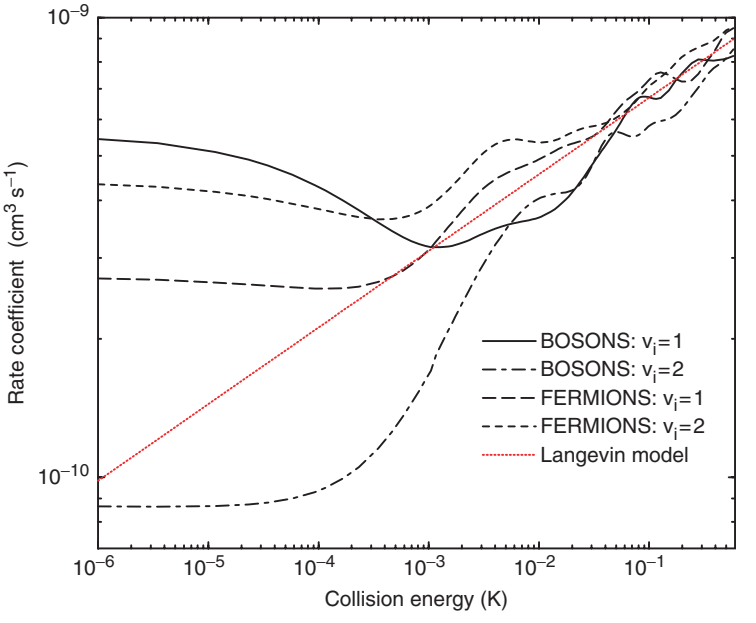

Figure 7. [Colour online] Total inelastic rate coefficients for collisions of Li with Li_2 ($v=1$ and 2, with $j=0$ for bosons and $j=1$ for fermions). Reproduced from Cvitaš *et al.* [35].

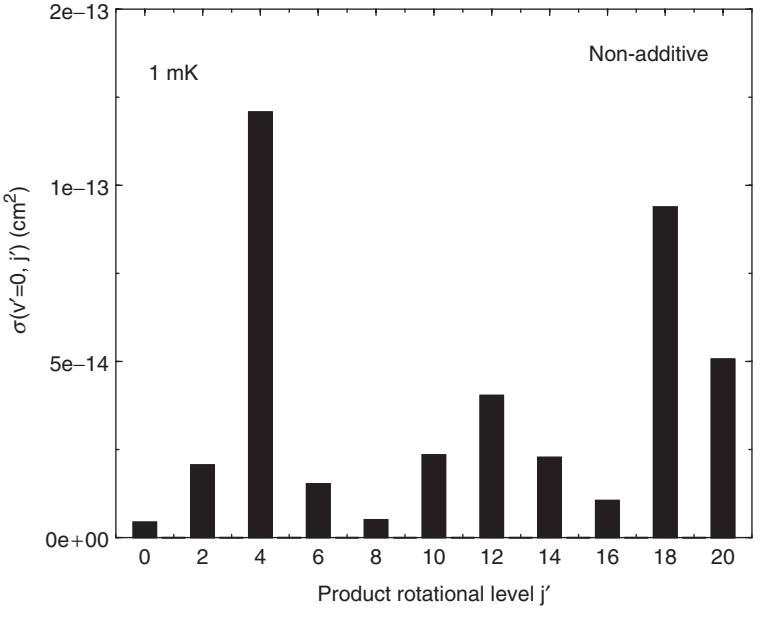

Figure 8. Rotational distributions for $^{23}Na + {}^{23}Na_2$ ($v=1$) at collision energy 10^{-4} K. The label j' is the final rotational quantum number of $^{23}Na_2$ ($v'=0$). Reproduced from Soldán *et al.* [46].

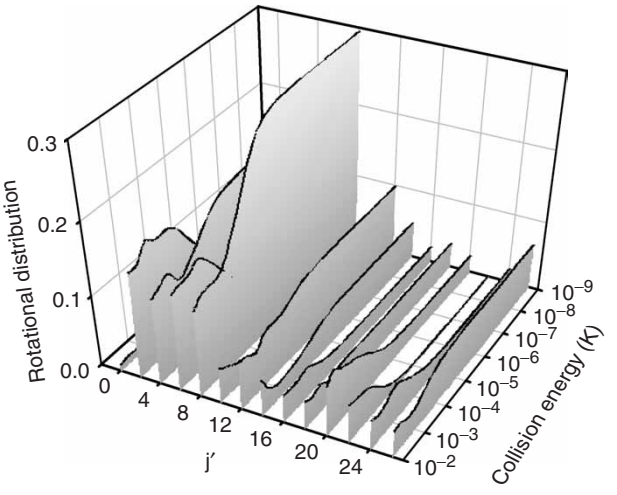

Figure 9. Rotational distributions for $^{39}K + {}^{39}K_2$ ($v = 1$) as a function of the collision energy. The label j' is the final rotational quantum number of $^{39}K_2$ ($v' = 0$). Reproduced from Quéméner *et al.* [51].

$j = 24$ are energetically accessible. Once again there is an oscillatory structure in the product state distributions.

5.5. *Potential sensitivity*

The sensitivity of the cross sections to details of the potential energy surface is of great importance. Soldán *et al.* [46] showed that including the non-additive part of the interaction potential changed both elastic and inelastic cross sections for $Na + Na_2$ ($v = 1$) by more than a factor of 10. Quéméner *et al.* [48] investigated this in more detail: they introduced a scaling factor λ to multiply the non-additive term, so that $\lambda = 0$ corresponds to a pairwise-additive potential and $\lambda = 1$ to the full non-additive potential. They then investigated cross sections as a function of λ for initial $v = 1$, 2 and 3. They found that elastic and inelastic cross sections varied by a factor of 10 for $v = 1$ for variations of λ as small as 0.01 either side of $\lambda = 1$. However, the variations became considerably smaller for $v = 2$ and 3. Cvitaš *et al.* [49] have investigated similar effects for $Li + Li_2$ at rather higher energy resolution. For $v = 0$, the elastic cross sections show very sharp structure as a function of λ as shown in figure 10, caused by poles in the scattering length each time there is a bound state at zero energy. However, the structure for $v > 0$ is weaker for both elastic and inelastic cross sections as shown in figure 11. This is due to a general effect discussed by Hutson [99]: in the presence of inelastic scattering, the poles in scattering lengths at the positions of zero-energy resonances are suppressed, and the suppression increases with the degree of inelastic scattering.

5.6. *Differential cross sections*

At very low energies, cross sections are completely dominated by the $l = 0$ partial wave. Under these circumstances, the scattering is completely isotropic and the differential

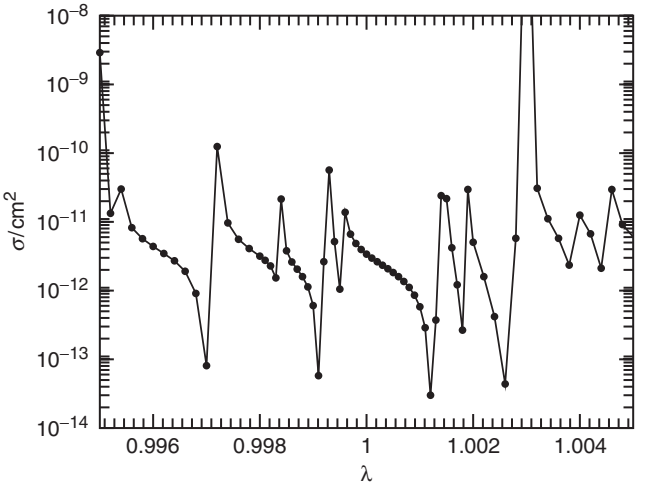

Figure 10. Dependence of the elastic cross sections for $^7Li + {}^7Li_2(v_i = 0, j_i = 0)$ at $E = 0.928$ nK on the scaling factor λ of the non-additive part of the potential. Reproduced from Cvitaš *et al*. [49].

cross sections are featureless. However, as the energy increases and higher partial waves start to contribute, angular structure appears. Low-energy scattering thus offers the opportunity to study the onset of angular behaviour in reactive cross sections. The way that the angular behaviour develops is shown for $K + K_2$ ($v = 1$) in figure 12. At 1 μK the scattering is completely isotropic, but for 100 μK some angular structure arising from interference between $l = 0$ and 1 is evident. At 0.1 mK partial waves up to $l = 5$ contribute and several peaks emerge.

5.7. *Heteronuclear molecules*

Heteronuclear molecules are particularly interesting because they offer the possibility of studying *reactive* collisions separately from inelastic collisions. Homonuclear molecules that are formed in their lowest vibration–rotation state are stable to collisions. For heteronuclear molecules, however, the situation is more complicated. Even molecules in their ground rovibrational states may not be stable against collisions. For example, the spin-polarized reaction

$$^6Li^7Li(v = 0, j = 0) + {}^7Li \rightarrow {}^6Li + {}^7Li_2(v = 0, j = 0) \tag{15}$$

is exothermic by 1.822 K because of the difference between the zero-point energies of the two dimers. However, the process

$$^6Li^7Li(v = 0, j = 0) + {}^6Li \rightarrow {}^7Li + {}^6Li_2(v = 0, j = 1) \tag{16}$$

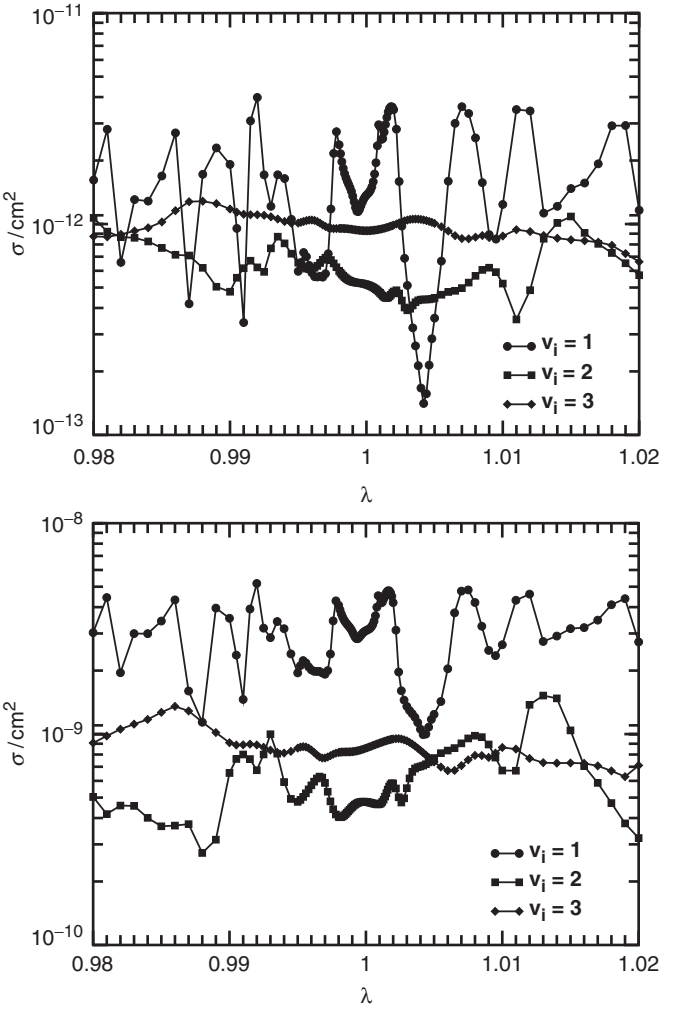

Figure 11. Dependence of the total elastic (upper panel) and inelastic (lower panel) cross sections for $^7Li + {}^7Li_2(v_i, j_i = 0)$ for $v_i = 1$, 2 and 3 and $E = 0.928$ nK on the scaling factor λ of the non-additive part of the potential. Reproduced from Cvitaš *et al.* [49].

cannot occur at collision energies below 2.643 K because of the combined effects of zero-point energy and the need to form $^6Li_2$ in $j = 1$ or higher to satisfy fermion symmetry requirements.

Cvitaš *et al.* [50] have investigated the process (15) and the resulting elastic and reactive cross sections are shown in figure 13. It may be seen that the reactive scattering dominates over elastic scattering below 10 μ*K*. The low-temperature reactive rate coefficient is only $4.7 \times 10^{-12}\,cm^3\,s^{-1}$, which is reduced by a factor of about 50 from those typical for vibrational relaxation in the homonuclear case. Cvitaš *et al.* attributed the difference to the fact that there is only a single open channel for reaction (15).

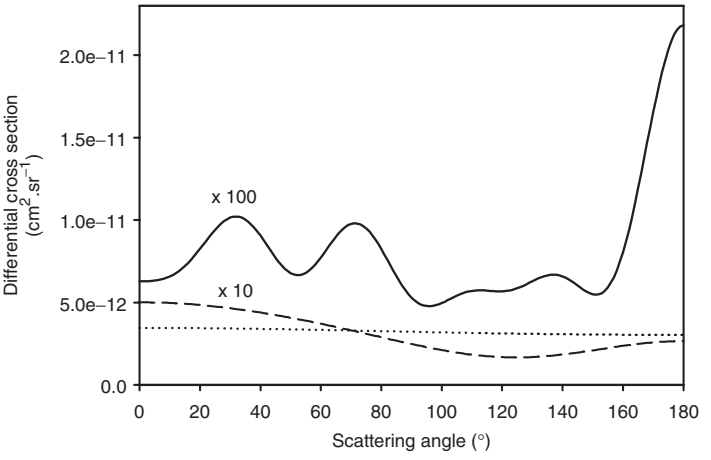

Figure 12. Differential cross section for inelastic scattering of $K + K_2$ ($v = 1$) at 1 μK (dotted line), 100 μK (dashed line) and 0.1 mK (solid line). Reproduced from Quéméner *et al.* [51]

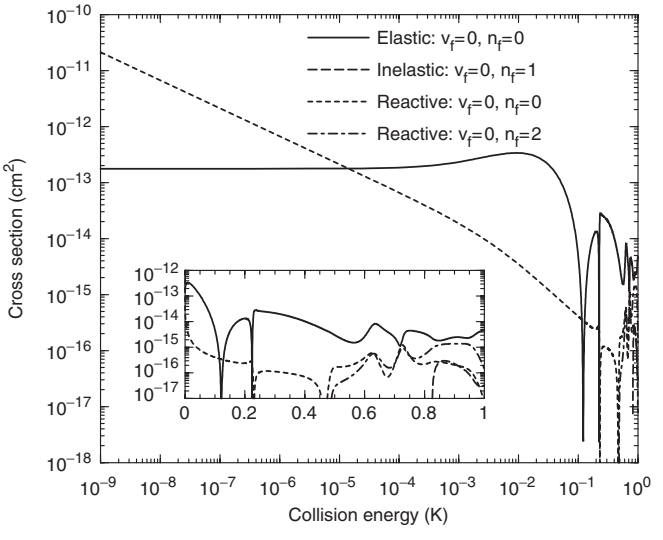

Figure 13. Elastic and reactive s-wave cross sections for $^7Li + {}^6Li^7Li(v = 0, j = 0)$. The inset shows the higher-energy cross sections on a log-linear scale, with axes in the same units as the main plot. Reproduced from Cvitaš *et al.* [50].

The results obtained in [50] have important implications. There is interest in producing a quantum gas of $^6Li^7Li$ in its ground rovibronic state in an ultracold mixture of ^6Li and ^7Li atoms. In order to stabilize the molecular cloud against two-body trap losses induced by the reactive process (15), the remaining atomic ^7Li would have to be removed quickly after ground-state molecule production, so that just the two-species fermionic mixture of $^6Li^7Li(v = 0, j = 0)$ molecules and ^6Li atoms is left in the trap.

The ^{6}Li cloud could be removed as well, but it might be advantageous to keep it in the trap. Elastic s-wave collisions between fermionic ^{6}Li^{7}Li molecules will be strongly suppressed, but low-energy collisions with ^{6}Li can result only in elastic scattering and might be used to achieve sympathetic cooling of the molecules.

5.8. *Further extensions*

Our work on the quantum dynamics of collisions of alkali metal dimers has so far been restricted in several ways. We have focussed on collisions of molecules in low vibrational states, for systems involving three chemically equivalent atoms. We have restricted ourselves to collisions of spin-stretched atoms and molecules, for which doublet electronic states do not contribute. We have neglected hyperfine structure, and worked in zero applied field.

Extending the calculations to handle heteronuclear systems is relatively straightforward, though a considerable amount of work is needed to develop potential energy surfaces for each system of interest. Dynamical calculations are more expensive for heavier atoms and for systems of lower symmetry (and the calculations described here already push the limits of current computers). Extending the calculations to higher vibrational states is also mostly a matter of computer time, though true long-range states very near dissociation may be difficult or impossible to converge with our current scattering methods.

Including the effects of nuclear spin and magnetic fields is a very difficult task, though an important one if we are to explore atom–molecule Feshbach resonances and use them to control molecular interactions in the same way as atomic interactions. Collisions of atoms and molecules in non-spin-stretched states will be particularly challenging, because they will involve doublet surfaces as well as quartet surfaces, and for alkali metal trimers the doublet surfaces exhibit conical intersections and geometric phase effects [100, 101] that considerably complicate the dynamics.

6. Conclusions

This article focussed on theoretical studies of collisions between spin-polarized alkali metal dimers and atoms, which are crucial in experiments designed to form ultracold molecules in low-lying vibrational states. Colliding dimers can undergo very fast barrierless chemical reactions. As a result, vibrationally excited molecules undergo very fast vibrational relaxation, with rates usually in excess of $k_{\mathrm{inel}} = 10^{-10}\,\mathrm{cm^3\,s^{-1}}$. At temperatures above about 1 mK, where several partial waves contribute, the rates are approximately given by a statistical Langevin capture model. At lower temperatures, however, the reactions enter a regime governed by Wigner threshold laws and a full quantum-dynamical treatment is essential to calculate the rates. In this regime the results are very sensitive to details of the triatomic potential energy surfaces, though the sensitivity decreases for excited vibrational levels. Isotopically heteronuclear molecules can often undergo exothermic reactions even from their ground vibrational states, because of the difference in zero-point energy between reactants and products.

Prospects for the future include the production of quantum-degenerate gases of ground-state molecules, which will be stable to collisions and offer a wealth of new possibilities for quantum control. Heteronuclear molecules are particularly interesting, because they can have substantial dipole moments in short-range states. Dipolar quantum gases offer a new range of novel properties, and ultracold polar molecules also have potential applications in quantum computing and in studying fundamental physical properties such as parity violation and the electron dipole moment.

Acknowledgments

PS acknowledges support from the Ministry of Education of the Czech Republic (grant no. LC06002).

References

[1] J. D. Weinstein, R. deCarvalho, T. Guillet, B. Friedrich, and J. M. Doyle, Nature **395**, 148 (1998).
[2] D. Egorov, W. C. Campbell, B. Friedrich, S. E. Maxwell, E. Tsikata, L. D. van Buuren, and J. M. Doyle, Eur. Phys. J. D **31**, 307 (2004).
[3] H. L. Bethlem and G. Meijer, Int. Rev. Phys. Chem. **22**, 73 (2003).
[4] H. L. Bethlem, M. R. Tarbutt, J. Küpper, D. Carty, K. Wohlfart, E. A. Hinds, and G. Meijer, J. Phys. B – At. Mol. Opt. Phys. **39**, R263 (2006).
[5] J. M. Hutson and P. Soldán, Int. Rev. Phys. Chem. **25**, 497 (2006).
[6] K. M. Jones, E. Tiesinga, P. D. Lett, and P. S. Julienne, Rev. Mod. Phys. **78**, 483 (2006).
[7] T. Köhler, K. Góral, and P. S. Julienne, Rev. Mod. Phys. **78**, 1311 (2006).
[8] S. Jochim, M. Bartenstein, A. Altmeyer, G. Hendl, S. Riedl, C. Chin, J. H. Denschlag, and R. Grimm, Science **302**, 2101 (2003).
[9] M. W. Zwierlein, C. A. Stan, C. H. Schunck, S. M. F. Raupach, S. Gupta, Z. Hadzibabic, and W. Ketterle, Phys. Rev. Lett. **91**, 250401 (2003).
[10] M. Greiner, C. A. Regal, and D. S. Jin, Nature **426**, 537 (2003).
[11] T. Kraemer, M. Mark, P. Waldburger, J. G. Danzl, C. Chin, B. Engeser, A. D. Lange, K. Pilch, A. Jaakkola, H. C. Nägerl, *et al*., Nature **440**, 315 (2006).
[12] C. Chin, T. Kraemer, M. Mark, J. Herbig, P. Waldburger, H. C. Näagerl and R. Grimm, Phys. Rev. Lett. **94**, 123201 (2005).
[13] J. J. Hudson, B. E. Sauer, M. R. Tarbutt, and E. A. Hinds, Phys. Rev. Lett. **89**, 023003 (2002).
[14] M. Quack and J. Stohner, Chimia **59**, 530 (2005).
[15] J. Crassous, C. Chardonnet, T. Saue, and P. Schwerdtfeger, Org. Biomol. Chem. **3**, 2218 (2005).
[16] E. R. Hudson, H. J. Lewandowski, B. C. Sawyer, and J. Ye, Phys. Rev. Lett. **96**, 143004 (2006).
[17] D. DeMille, Phys. Rev. Lett. **88**, 067901 (2002).
[18] M. Baranov, Ł. Dobrek, K. Góral, L. Santos, and M. Lewenstein, Phys. Scr. **T102**, 74 (2002).
[19] R. V. Krems, Int. Rev. Phys. Chem. **24**, 99 (2005).
[20] E. Bodo and F. A. Gianturco, Int. Rev. Phys. Chem. **25**, 313 (2006).
[21] P. F. Weck and N. Balakrishnan, Int. Rev. Phys. Chem. **25**, 283 (2006).
[22] E. A. Donley, N. R. Claussen, S. T. Thompson, and C. E. Wieman, Nature **417**, 529 (2002).
[23] J. Herbig, T. Kraemer, M. Mark, T. Weber, C. Chin, H. C. Nägerl and R. Grimm, Science **301**, 1510 (2003).
[24] K. Xu, T. Mukaiyama, J. R. Abo-Shaeer, J. K. Chin, D. E. Miller, and W. Ketterle, Phys. Rev. Lett. **91**, 210402 (2003).
[25] S. Dürr, T. Volz, A. Marte, and G. Rempe, Phys. Rev. Lett. **92**, 020406 (2004).
[26] S. T. Thompson, E. Hodby, and C. E. Wieman, Phys. Rev. Lett. **94**, 020401 (2005).
[27] T. Köhler, E. Tiesinga, and P. S. Julienne, Phys. Rev. Lett. **94**, 020402 (2005).
[28] T. Mukaiyama, J. R. Abo-Shaeer, K. Xu, J. K. Chin, and W. Ketterle, Phys. Rev. Lett. **92**, 180402 (2004).
[29] K. E. Strecker, G. B. Partridge, and R. G. Hulet, Phys. Rev. Lett. **91**, 080406 (2003).

[30] J. Cubizolles, T. Bourdel, S. J. J. M. F. Kokkelmans, G. V. Shlyapnikov, and C. Salomon, Phys. Rev. Lett. **91**, 240401 (2003).
[31] S. Jochim, M. Bartenstein, A. Altmeyer, G. Hendl, C. Chin, J. H. Denschlag, and R. Grimm, Phys. Rev. Lett. **91**, 240402 (2003).
[32] C. A. Regal, M. Greiner, and D. S. Jin, Phys. Rev. Lett. **92**, 083201 (2004).
[33] D. S. Petrov, C. Salomon, and G. V. Shlyapnikov, Phys. Rev. Lett. **93**, 090404 (2004).
[34] D. S. Petrov, C. Salomon, and G. V. Shlyapnikov, Phys. Rev. A **71**, 012708 (2005).
[35] M. T. Cvitaš, P. Soldán, J. M. Hutson, P. Honvault, and J. M. Launay, Phys. Rev. Lett. **94**, 033201 (2005).
[36] R. Wynar, R. S. Freeland, D. J. Han, C. Ryu, and D. J. Heinzen, Science **287**, 1016 (2000).
[37] P. Staanum, S. D. Kraft, J. Lange, R. Wester, and M. Weidemüller, Phys. Rev. Lett. **96**, 023201 (2006).
[38] N. Zahzam, T. Vogt, M. Mudrich, D. Comparat, and P. Pillet, Phys. Rev. Lett. **96**, 023202 (2006).
[39] D. Jaksch, V. Venturi, J. I. Cirac, C. J. Williams, and P. Zoller, Phys. Rev. Lett. **89**, 040402 (2002).
[40] C. P. Koch, J. P. Palao, R. Kosloff, and F. Masnou-Seeuws, Phys. Rev. A **70**, 013402 (2004).
[41] C. P. Koch, E. Luc-Koenig, and F. Masnou-Seeuws, Phys. Rev. A **73**, 033408 (2006).
[42] W. Salzmann, U. Poschinger, R. Wester, M. Weidemüller, A. Merli, S. M. Weber, F. Sauer, M. Plewicki, F. Weise, A. M. Esparza, *et al*., Phys. Rev. A **73**, 023414 (2006).
[43] H. Wang and W. C. Stwalley, J. Chem. Phys. **108**, 5767 (1998).
[44] W. C. Stwalley, Eur. Phys. J. D **31**, 221 (2004).
[45] J. M. Sage, S. Sainis, T. Bergeman, and D. DeMille, Phys. Rev. Lett. **94**, 203001 (2005).
[46] P. Soldán, M. T. Cvitaš, J. M. Hutson, P. Honvault, and J. M. Launay, Phys. Rev. Lett. **89**, 153201 (2002).
[47] P. Soldán, M. T. Cvitaš, and J. M. Hutson, Phys. Rev. A **67**, 054702 (2003).
[48] G. Quéméner, P. Honvault, and J. M. Launay, Eur. Phys. J. D **30**, 201 (2004).
[49] M. T. Cvitaš, P. Soldán, J. M. Hutson, P. Honvault, and J. M. Launay, in preparation (2007).
[50] M. T. Cvitaš, P. Soldán, J. M. Hutson, P. Honvault, and J. M. Launay, Phys. Rev. Lett. **94**, 200402 (2005).
[51] G. Quéméner, P. Honvault, and J. M. Launay, Phys. Rev. A **71**, 032722 (2005).
[52] M. T. Cvitaš, P. Soldán, and J. M. Hutson, Mol. Phys. **104**, 23 (2006).
[53] M. D. Halls, H. B. Schlegel, M. J. DeWitt, and G. W. F. Drake, Chem. Phys. Lett. **339**, 427 (2001).
[54] B. Minaev, Spectroc. Acta Pt. A – Molec. Biomolec. Spectr. **62**, 790 (2005).
[55] V. S. Ivanov, V. B. Sovkov, and L. Li, J. Chem. Phys. **118**, 8242 (2003).
[56] E. Ahmed, A. M. Lyyra, F. Xie, D. Li, Y. Chu, L. Li, V. S. Ivanov, V. B. Sovkov, and S. Magnier, J. Mol. Spectrosc. **234**, 41 (2005).
[57] B. D. Esry, C. H. Greene, and J. P. Burke, Phys. Rev. Lett. **83**, 1751 (1999).
[58] H. Suno, B. D. Esry, C. H. Greene, and J. P. Burke, Phys. Rev. A **65**, 042725 (2002).
[59] H. Suno, B. D. Esry, and C. H. Greene, Phys. Rev. Lett. **90**, 053202 (2003).
[60] H. Suno, B. D. Esry, and C. H. Greene, New J. Phys. **5**, 53 (2003).
[61] J. Higgins, T. Hollebeek, J. Reho, T. S. Ho, K. K. Lehmann, H. Rabitz, G. Scoles, and M. Gutowski, J. Chem. Phys. **112**, 5751 (2000).
[62] P. J. Knowles, C. Hampel, and H. J. Werner, J. Chem. Phys. **99**, 5219 (1993).
[63] J. Čížek, J. Chem. Phys. **45**, 4256 (1966).
[64] S. F. Boys and F. Bernardi, Mol. Phys. **19**, 553 (1970).
[65] H.-J. Werner, P. J. Knowles, R. Lindh, M. Schütz, P. Celani, T. Korona, F. R. Manby, G. Rauhut, R. D. Amos, A. Bernhardsson, *et al*., Molpro, version 2002.6, a package of ab initio programs, 2003, see http://www.molpro.net.
[66] I. Røeggen and J. Almlöf, J. Chem. Phys. **102**, 7095 (1995).
[67] V. F. Lotrich and K. Szalewicz, J. Chem. Phys. **106**, 9688 (1997).
[68] B. M. Axilrod and E. Teller, J. Chem. Phys. **11**, 299 (1943).
[69] Y. Muto, Proc. Phys. Math. Soc. Japan **17**, 629 (1943).
[70] F. D. Colavecchia, F. Mrugała, G. A. Parker, and R. T Pack, J. Chem. Phys. **118**, 10387 (2003).
[71] W. L. Bade, J. Chem. Phys. **27**, 1280 (1957).
[72] W. L. Bade, J. Chem. Phys. **28**, 282 (1958).
[73] R. J. Bell, J. Phys. B – At. Mol. Phys. **3**, 751 (1970).
[74] M. B. Doran and I. J. Zucker, J. Phys. C – Solid State Phys. **4**, 307 (1971).
[75] T. S. Ho and H. Rabitz, J. Chem. Phys. **104**, 2584 (1996).
[76] T. S. Ho and H. Rabitz, J. Chem. Phys. **113**, 3960 (2000).
[77] P. Soldán and J. M. Hutson, J. Chem. Phys. **112**, 4415 (2000).
[78] D. A. Brue, X. Li, and G. A. Parker, J. Chem. Phys. **123**, 091101 (2005).
[79] S. C. Althorpe and D. C. Clary, Annu. Rev. Phys. Chem. **54**, 493 (2003).
[80] S. C. Althorpe, Int. Rev. Phys. Chem. **23**, 219 (2004).

[81] D. Skouteris, J. F. Castillo, and D. E. Manolopoulos, Comput. Phys. Commun. **133**, 128 (2000).
[82] N. Balakrishnan and A. Dalgarno, Chem. Phys. Lett. **341**, 652 (2001).
[83] E. Bodo, F. A. Gianturco, and A. Dalgarno, J. Chem. Phys. **116**, 9222 (2002).
[84] E. Bodo, F. A. Gianturco, N. Balakrishnan, and A. Dalgarno, J. Phys. B – At. Mol. Opt. Phys. **37**, 3641 (2004).
[85] P. F. Weck and N. Balakrishnan, J. Chem. Phys. **123**, 144308 (2005).
[86] R. C. Whitten and F. T. Smith, J. Math. Phys. **9**, 1103 (1968).
[87] R. T Pack and G. A. Parker, J. Chem. Phys. **87**, 3888 (1987).
[88] G. A. Parker, R. T Pack, B. J. Archer, and R. B. Walker, Chem. Phys. Lett. **137**, 564 (1987).
[89] B. D. Esry, C. D. Lin, and C. H. Greene, Phys. Rev. A **54**, 394 (1996).
[90] J. M. Launay and M. LeDourneuf, Chem. Phys. Lett. **163**, 178 (1989).
[91] P. Honvault and J. M. Launay, J. Chem. Phys. **111**, 6665 (1999).
[92] P. Honvault and J. M. Launay, J. Chem. Phys. **114**, 1057 (2001).
[93] A. M. Arthurs and A. Dalgarno, Proc. Roy. Soc., Ser. A **256**, 540 (1960).
[94] H. R. Sadeghpour, J. L. Bohn, M. J. Cavagnero, B. D. Esry, I. I. Fabrikant, J. H. Macek, and A. R. P. Rau, J. Phys. B – At. Mol. Opt. Phys. **33**, R93 (2000).
[95] R. D. Levine and R. B. Bernstein, *Molecular Reaction Dynamics and Chemical Reactivity*, Oxford University Press, 1987.
[96] J. M. Bowman, Chem. Phys. Lett. **62**, 309 (1979).
[97] R. Schinke and P. McGuire, J. Chem. Phys. **71**, 4201 (1979).
[98] J. M. Hutson, C. J. Ashton, and R. J. Le Roy, J. Phys. Chem. **87**, 2713 (1983).
[99] J. M. Hutson, arXiv:physics/0610210 (2006).
[100] B. K. Kendrick, J. Phys. Chem. A **107**, 6739 (2003).
[101] S. C. Althorpe, J. Chem. Phys. **124**, 084105 (2006).